Wetland Mapping in Great Lakes Using Sentinel-1/2 Time-Series Imagery and DEM Data in Google Earth Engine

Downloaded from: https://research.chalmers.se, 2026-04-04 15:07 UTC

Citation for the original published paper (version of record):

Mohseni, F., Amani, M., Mohammadpour, P. et al (2023). Wetland Mapping in Great Lakes Using Sentinel-1/2 Time-Series Imagery and DEM Data in Google Earth Engine. Remote Sensing, 15(14). http://dx.doi.org/10.3390/rs15143495

N.B. When citing this work, cite the original published paper.

research.chalmers.se offers the possibility of retrieving research publications produced at Chalmers University of Technology. It covers all kind of research output: articles, dissertations, conference papers, reports etc. since 2004. research.chalmers.se is administrated and maintained by Chalmers Library

(article starts on next page)

remote sensing

MDPI

Article

Wetland Mapping in Great Lakes Using Sentinel-1/2 Time-Series Imagery and DEM Data in Google Earth Engine

Farzane Mohseni [1], Meisam Amani [2,3,*], Pegah Mohammadpour [4,5], Mohammad Kakooei [6], Shuanggen Jin [2,7] and Armin Moghimi [8]

1 Institute of Geodesy and Geoinformation, University of Bonn, 53115 Bonn, Germany; mohseni@igg.uni-bonn.de
2 School of Surveying and Land Information Engineering, Henan Polytechnic University, Jiaozuo 454000, China; sgjin@shao.ac.cn
3 WSP Environment and Infrastructure Canada Limited, Ottawa, ON K2E 7L5, Canada
4 Univ of Coimbra, ADAI, Department of Mechanical Engineering, Rua Luís Reis Santos, Pólo II, 3030-788 Coimbra, Portugal; pegah@adai.pt
5 Universidad de Alcala, Environmental Remote Sensing Research Group, Department of Geology, Geography and Environment, Colegios 2, 28801 Alcalá de Henares, Spain
6 Department of Computer Science, Chalmers University of Technology, Rännvägen 6, 41258 Gothenburg, Sweden; kakooei@chalmers.se
7 Shanghai Astronomical Observatory, Chinese Academy of Sciences, Shanghai 200030, China
8 Ludwig-Franzius Institute of Hydraulic, Estuarine and Coastal Engineering, Leibniz University Hannover, Nienburger Str. 4, 30167 Hannover, Germany; moghimi@lufi.uni-hannover.de
* Correspondence: meisam.amani@wsp.com

Abstract: The Great Lakes (GL) wetlands support a variety of rare and endangered animal and plant species. Thus, wetlands in this region should be mapped and monitored using advanced and reliable techniques. In this study, a wetland map of the GL was produced using Sentinel-1/2 datasets within the Google Earth Engine (GEE) cloud computing platform. To this end, an object-based supervised machine learning (ML) classification workflow is proposed. The proposed method contains two main classification steps. In the first step, several non-wetland classes (e.g., Barren, Cropland, and Open Water), which are more distinguishable using radar and optical Remote Sensing (RS) observations, were identified and masked using a trained Random Forest (RF) model. In the second step, wetland classes, including Fen, Bog, Swamp, and Marsh, along with two non-wetland classes of Forest and Grassland/Shrubland were identified. Using the proposed method, the GL were classified with an overall accuracy of 93.6% and a Kappa coefficient of 0.90. Additionally, the results showed that the proposed method was able to classify the wetland classes with an overall accuracy of 87% and a Kappa coefficient of 0.91. Non-wetland classes were also identified more accurately than wetlands (overall accuracy = 96.62% and Kappa coefficient = 0.95).

Keywords: Great Lakes; wetlands; remote sensing; Google Earth Engine; random forest classification

check for updates

Citation: Mohseni, F.; Amani, M.; Mohammadpour, P.; Kakooei, M.; Jin, S.; Moghimi, A. Wetland Mapping in Great Lakes Using Sentinel-1/2 Time-Series Imagery and DEM Data in Google Earth Engine. *Remote Sens.* **2023**, *15*, 3495. https://doi.org/10.3390/rs15143495

Academic Editors: Gaofei Yin, Jean-Philippe Gastellu-Etchegorry, Baodong Xu and Shengbiao Wu

Received: 7 June 2023
Revised: 5 July 2023
Accepted: 5 July 2023
Published: 11 July 2023

Copyright: © 2023 by the authors. Licensee MDPI, Basel, Switzerland. This article is an open access article distributed under the terms and conditions of the Creative Commons Attribution (CC BY) license (https://creativecommons.org/licenses/by/4.0/).

1. Introduction

Wetlands have significant impacts on a variety of plant and animal species, ecosystem dynamics, the energy exchange between the atmosphere and soil, and terrestrial biodiversity [1]. Despite their ecological significance, wetlands have been degraded as a result of agricultural activities, construction projects, population growth, and natural processes such as global warming, precipitation reduction, and coastal destruction [2,3]. Thus, wetland mapping and monitoring are critical, especially in developed countries that require adequate infrastructure for landscape planning, land and livestock management, and water resource management [4,5].

Although field-based measurements are the most accurate data for wetland monitoring, they are costly, labor-intensive, time-consuming, and associated with safety risks. The

availability of consistent archived and near-real-time satellite imagery, their reasonable spatial and temporal resolutions, and their global coverage have made remote sensing (RS) an important tool for wetland studies [6,7]. Over the last few decades, considerable advancements have been made in both algorithms and practical applications of wetland classification using RS datasets [8,9].

Wetland classification methods are usually divided into three groups: pixel-, sub-pixel-, and object-based techniques [10]. Pixel-based techniques, or per-pixel classification approaches, identify the best label for a pixel using different methods and cost functions [11,12]. Sub-pixel-based methods have been established to overcome one of the main restrictions of pixel-based approaches, namely the spectral blending problem. This problem is mainly encountered in medium and coarse spatial resolution RS images [13]. Usually, both pixel- and sub-pixel-based classification methods identify the labels of the pixels or sub-pixels using their spectral features without considering their particular location or their neighbors in the image. However, object-based classification methods consider both the spectral and spatial characteristics of a group of pixels [14,15]. Briefly, in object-based classification approaches, pixels are first grouped into specific objects (i.e., segments) using an image segmentation algorithm. The segments are then classified based on the average values of the defined features of each segment [16]. For all three groups of classification approaches, the spatial resolution of the satellite imagery, number of spectral bands, repetition time of the RS datasets, and complexity of the study area have direct effects on the precision of the final classified wetlands [11]. Overall, it has been frequently reported that using object-based classification techniques improves the accuracy of the classified map, particularly when using high-resolution RS datasets [8,12,17–19].

Classification techniques are also divided into unsupervised and supervised algorithms, depending on the approach used to identify different types of land covers. In unsupervised classification algorithms, the objects/pixels of an input image are classified into a set of classes based on the statistical criteria of the image, without utilizing prior knowledge of the area [20]. A supervised classification method, on the other hand, is based on prior knowledge about the classes of some pixels in the image (training samples). In this method, a suitable number of pixels with known labels are first selected as training samples. Then, other pixels in the image are classified based on their spectral properties and the developing classification decision rules [21]. Some of the most well-known supervised classification methods are the Maximum Likelihood Classifier (MLC), Artificial Neural Network (ANN), Decision Tree (DT), Boosted DT (BDT), Random Forests (RF), Support Vector Machine (SVM), k-Nearest Neighbor (k-NN), and Genetic Algorithms (GA). Among the various supervised and unsupervised classification methods, Machine Learning (ML) methods have become a prominent focus of RS for wetland mapping [22]. It has been widely reported that among different ML classification techniques, RF achieves better performance for wetland mapping [8,23–25].

Researchers have also shown that Sentinel-1/2 and Landsat satellite data are among the most popular RS data for wetland studies [7,8]. This is mainly due to their open access policy and relatively suitable spatial, spectral, and temporal resolutions. However, processing and analyzing large geospatial datasets over large areas using commonly used software packages is time-consuming and not efficient in terms of computation cost [26–28]. To overcome this problem, cloud computing platforms with large computational capacities, such as Amazon's Web Services, NASA Earth Exchange, Google Earth Engine (GEE), and Microsoft's Azure, have been developed [29,30].

GEE is a cloud-based computing platform that includes massive amounts of open access earth observation datasets, image processing, and classification algorithms [25,30]. The availability of many datasets and ready-to-use image-driven products, easy downloading and uploading of data in various formats, and access to many image processing and ML algorithms are some of the features that have contributed to the widespread use of GEE [30–33].

So far, numerous studies have mapped vast wetland areas using GEE. For instance, Hird et al. [34] used GEE to develop a model predicting the probability of wetland occurrence in a 13,700 km^2 study area in northern Alberta. They applied a strengthened Boosted Regression Tree (BRT) model using various RS datasets. Results showed that high-quality topographic variables, along with optical and radar variables, significantly improved the model's performance in mapping wetland distribution, achieving a best overall accuracy of 85%. McCarthy et al. [35] proposed a method for mapping large-scale forested wetland, upland, cultivated land, un-vegetated land, and water in a 6500 km^2 watershed using WorldView-2 satellite imagery. Their method identified forested wetlands and uplands with an overall accuracy of 78% and 64%, respectively. Additionally, Amani et al. [26] used GEE to process around 30,000 Landsat-8 data and generated the first wetland map of Canada. They utilized the RF classification approach to classify wetlands into five major classes defined by the Canadian Wetland Classification System (CWCS), including shallow Water, Marsh, Swamp, Fen, and Bog.

To monitor and map the coastal wetlands of China, Wang et al. [36] used GEE and 2798 Landsat images (ETM+/OLI) from 2018. They proposed a new pixel- and phenology-based algorithm to classify a wetland area of 7474.6 km^2, including tidal, evergreen, and deciduous wetlands. The results showed the high potential of GEE, with the highest overall accuracy of 98%, for coastal wetland classification at large scales. Furthermore, Mahdianpari et al. [37] produced a 10 m spatial resolution map of wetlands in Canada using Sentinel-1 and Sentinel-2 images within GEE. For this purpose, they developed an object-based RF method using a large number of reference samples within GEE, resulting in an individual accuracy of 74% to 84% depending on the province. Ghorbanian et al. [38] also developed a pixel-based RF algorithm in GEE to map the mangrove ecosystem using a combination of Sentinel-1/2 datasets. Additionally, Fekri et al. [39] developed a RF algorithm and an automatic change detection method in GEE to map and identify changes in the International Shadegan Wetland (ISW) areas in southwestern Iran from 2018 to 2021 using a combination of Sentinel-1 and Sentinel-2 data. Finally, DeLancey et al. [40] used Sentinel-2 imagery from 2017 to 2020 in GEE to monitor the seasonal flooding dynamics of wetlands in a prairie pothole wetland landscape in Alberta, Canada.

Among the previously mentioned studies on wetland classification and monitoring using RS data, there are some examples of publications that highlight wetland mapping and monitoring in the Great Lakes (GL) region using RS from both Canadian and American authors [9,41–43]. The GL, which are along the Canada–United States (US) border, contain a large number of wetland types [44]. The GL's wetlands support a variety of rare and endangered animal and plant species. Despite the astonishing amount of biodiversity and the ecohydrological importance of the wetlands of the GL, these ecosystems are under severe threat, mainly from climate change, as well as agricultural and urban growth [2,3]. For instance, the Michigan subbasin of the GL has lost about 50% of the coastal wetlands since European settlement [45]. Considering the population growth and wetland loss in the GL, it is highly required to develop accurate methods for wetland classification and monitoring in these regions. Previous efforts have focused only on the coast or on only one country. There are dozens of examples of case studies.

Despite numerous studies on the application of RS and GEE for large-scale wetland mapping, there is only one study [46] which has used Sentinel data in GEE to classify the GL into two major classes, overlooking the importance of differentiating wetland types and capturing the ecological diversity and functional differences within the region. Additionally, the broad grouping of upland land covers fails to account for the spatial heterogeneity and variability of upland areas, and the simplified classification scheme may not accurately represent the complex land cover patterns in the GL region. Moreover, the inability to address specific conservation and management needs for different land cover categories may hinder targeted efforts. This oversimplification could also have implications for environmental policies and decision making.

To address the aforementioned limitations, the objective of this research is to generate a more detailed and accurate 10 m resolution wetland map of the GL region within GEE based on the well-established CWCS. This objective was accomplished by utilizing the Sentinel-1 and Sentinel-2 datasets in conjunction with an object-based supervised ML algorithm. To achieve this goal, we focused on distinguishing between four wetland classes (Bog, Fen, Marsh, and Swamp) and five non-wetland classes (Open Water, Forest, Grassland/Shrubland, Cropland, and Barren). The GEE computing platform was also used for data access, preprocessing, implementing the proposed classification algorithm, and evaluating its accuracy. By adopting this approach, the study aims to achieve a more detailed and nuanced classification of wetland types while also improving the differentiation and characterization of upland land covers. The ultimate goal is to enhance the accuracy and utility of the wetland mapping results, which will provide valuable information for informed conservation and management efforts in the GL region.

2. Study Area and Data

2.1. Study Area

The study area was the GL region, which has a total area of 765,370 km^2 and is located between 93.7–73.9W and 40.5–50.8N (see Figure 1). The GL region consists of five interconnected freshwater lakes or sub-basins, including Superior, Michigan, Huron, Erie, and Ontario. The core of the GL region is located in the central-eastern part of North America and is connected to the Atlantic Ocean by the St. Lawrence River.

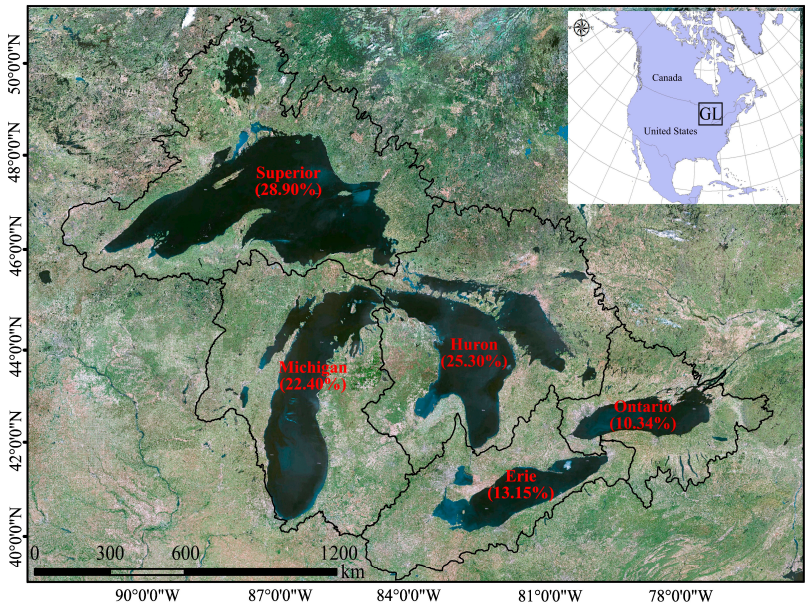

Figure 1. The spatial extent of the GL region and its five sub-basins (i.e., Superior, Michigan, Huron, Erie, and Ontario).

2.2. Field Data

Field samples of wetlands and non-wetlands were collected from different GL basins by various organizations, including the National Aeronautics and Space Administration (NASA), Michigan Tech Research Institute (MTRI), Dalhousie University (Dal), Environment and Climate Change Canada (ECCC), Ontario Parks (OP), and the Ministry of Northern Development, Mines, Natural Resources, and Forestry (NDMNRF). The primary purpose of providing these datasets was to allow researchers to monitor, assess, and analyze the number and types of wetlands in the GL region accurately, for a timely and cost-effective response to environmental problems. In this study, we used the corresponding datasets to train and evaluate the classification models. The numbers of polygon samples used in this study are provided in Table 2 for each class separately.

Table 1. Number (area/km^2) of polygon samples for the wetland and non-wetland classes collected by different organizations.

Class			MTRI [1]	NASA [2]	Dal [3]	ECCC [4]	OP [5]	NDMNRF [6]	This Study
Non-wetland classes	Barren		0	0	0	0	59 (4368.7)	24 (116.7)	1723 (3484.03)
	Cropland		12 (198.6)	0	0	0	364 (2829.5)	4 (37.0)	3967 (51,358.59)
	Open Water		155 (3775.2)	0	113 (51.0)	8 (1286.0)	0	20 (226.0)	1644 (28,893.95)
	Forest		43 (1043.8)	5 (46.2)	0	35 (617.9)	0	472 (13,491.6)	4603 (29,870.02)
	Grassland/Shrubland	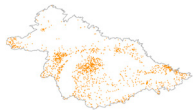	0	0	0	0	300 (1534.2)	2 (8.2)	4611 (30,738.90) For all Grassland/Shrubland, Bog, Fen, Marsh, and Swamp

Table 2. Number (area/km^2) of polygon samples for the wetland and non-wetland classes collected by different organizations.

Class			MTRI [1]	NASA [2]	Dal [3]	ECCC [4]	OP [5]	NDMNRF [6]	This Study
Wetland classes	Bog		59 (1125.0)	15 (112.1)	0	0	16 (68.2)	11 (122.4)	
	Fen		99 (5831.6)	17 (188.9)	0	0	0	30 (425.6)	
	Marsh		695 (13,314.7)	188 (834.6)	54 (88.7)	27 (1885.4)	0	116 (1309.2)	
	Swamp	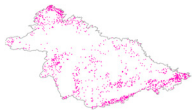	0	0	48 (782.1)	13 (1736.3)	0	211 (3835.8)	
	Total		1062 (25,284.6)	224 (1179.2)	215 (921.8)	83 (5525.6)	712 (8629.0)	890 (19,572.5)	16,548 (144,345.49)

[1] MTRI: Michigan Tech Research Institute; [2] NASA: National Aeronautics and Space Administration; [3] Dal: Dalhousie University; [4] ECCC: Environment and Climate Change Canada; [5] OP: Ontario Parks; [6] NDMNRF: Ministry of Northern Development, Mines, Natural Resources, and Forestry.

As shown in Table 2, almost half of the samples collected by MTRI, NASA, Dal, ECCC, OP, and NDMNRF belong to the wetland classes. However, it is expected that a large part of the study area shown in Figure 1 is covered by non-wetland classes. This issue can cause inaccuracies in classification. It is a basic principle of machine learning classification methods that the number and distribution of samples from different classes have a major impact on the output accuracy [22]. In this regard, the number of samples for each class should be balanced with the area covered by that class. For this reason, and to maintain balance between ground samples in different classes, we generated additional samples using high-resolution images from GEE. The number of these samples is also provided in the last column of Table 2. Given the classification method proposed and developed in this study (Section 3), samples were collected for five classes: Barren, Cropland, Open Water, Forest, and Other, including wetland classes and Grassland/Shrubland.

It is important to note that in addition to the four wetland species considered in this study, there are several other invasive species in the GL region, such as *Phragmites australis*, *Lythrum salicaria*, and *Typha angustifolia*, which are significant concerns for monitoring and studying GL wetlands. Although these invasive species are prevalent in the area, our study did not specifically focus on them due to the limitations of the existing dataset.

2.3. Satellite Data

Archived multitemporal Sentinel-1 and Sentinel-2 images from between 1 January 2020 and 1 January 2022, available on GEE (https://developers.google.com/earth-engine/datasets/catalog/sentinel, accessed on 6 July 2023), were used in this study. Additionally, Digital Elevation Models (DEMs) derived from Shuttle Radar Topography Mission (SRTM) data were combined with other multispectral and radar data to develop classification results (Figure 2).

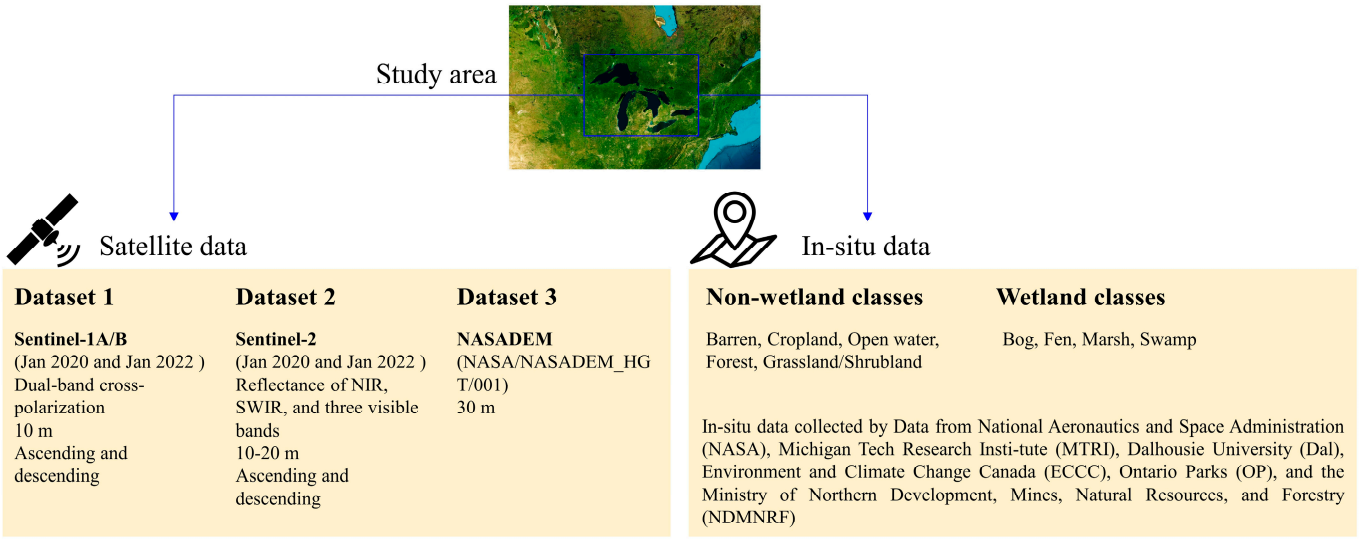

Figure 2. Satellite and in situ data applied in this study for wetland mapping in the GL region.

Using these datasets was mainly based on previous experience with classification methods. It has been widely reported that multitemporal imagery and the features extractable from them are the most useful RS data for wetland classification due to the dynamic characteristics of wetlands [47–49]. The radar backscattering coefficient also contributes to the accuracy of wetland classification [50]. Moreover, due to the difference in topography between wetlands, which are usually located in flat areas, and non-wetlands, DEM data also improve the classification results [51].

The Copernicus Sentinel-1A and Sentinel-1B C-band (5.405 GHz) radar mission providing all-weather and day and night data was developed by the European Space Agency

(ESA). Sentinel-1A and 1B observe the values of the backscattering coefficient at the multi-polarizations of vertical-vertical (VV), horizontal-horizontal (HH), HV, and VH at a temporal resolution of 6 days in both ascending and descending orbits [38]. In GEE, the interferometric wide swath (IW) mode of the ground range detected (GRD) of Sentinel-1 is processed and is available at one of three spatial resolutions of 10, 25, or 40 m and four possible band combinations, including single co-polarization VV, single co-polarization HH, dual-band cross-polarization VV + VH, and dual-band cross-polarization HH + HV. In this study, the ortho-corrected backscattering coefficient product of the dual-band cross-polarization VV + VH of Sentinel-1 at the spatial resolution of 10 m in both ascending and descending orbits was utilized.

Similar to the Sentinel-1 mission, the Sentinel-2 mission has been developed by the ESA to provide a spectral dataset over land and coastal waters [52,53]. Generally, Sentinel-2 is a wide-swath, multi-spectral, and multi-resolution imaging mission that observes in 13 different spectral bands: aerosols and water vapor (at 60 m spatial resolution); blue, green, red, and near-infrared (NIR at 10 m); four red-edge bands (at 20 m); and two shortwave infrared (SWIR at 20 m) bands [54]. In this study, three visible, NIR, and SWIR bands of Sentinel-2 were utilized.

The GEE database provides the reprocessed version of STRM data, enhanced by the auxiliary data from the ASTER GDEM, ICESat GLAS, and PRISM datasets (NASADEM). In NASADEM, the phase unwrapping is improved using ICESat GLAS data for controlling and reducing the voids. In this study, the NASADEM (NASA/NASADEM_HGT/001) with a spatial resolution of 30 m was utilized.

3. Methodology

Figure 3 schematically illustrates the proposed classification method for wetland mapping in the GL region. As shown in Figure 3, the proposed method had several steps, each of which is described in the following subsections.

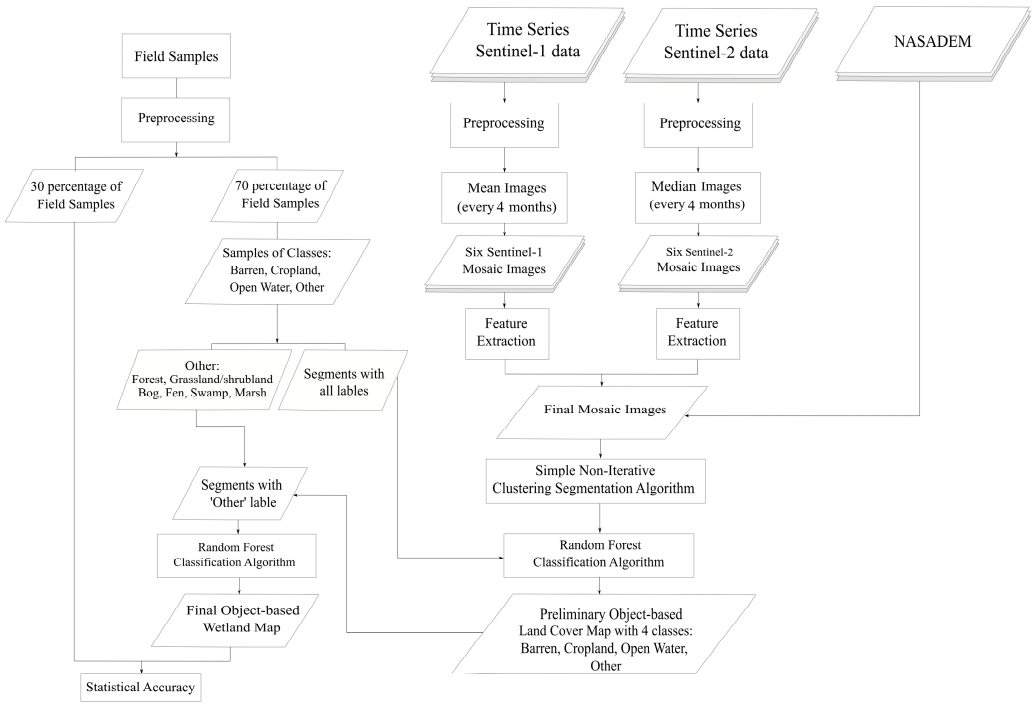

Figure 3. Flowchart of the proposed classification method for wetland mapping in GL using Sentinel-1/2 images and DEM data in GEE.

3.1. Data Preparation

The preprocessing step was applied to both in situ and RS datasets. Additionally, several features were extracted from the RS data for utilization in the classification model.

3.1.1. Field Data Preprocessing

All field samples were independently separated into two groups of training (70%) and testing (30%). Training and test data were randomly selected using GEE. All training samples were then reclassified into four classes of Barren, Open Water, Cropland, and Other. The Other class included samples of all wetland classes, Grassland/Shrubland, and Forest.

3.1.2. RS Data Preprocessing

Initially, all Sentinel-1 backscattering data and Sentinel-2 reflectance images were preprocessed. For the Sentinel-1 radar data, mean values were obtained every four months between January 2020 and January 2022 to reduce the effects of speckle noise, which is a common error in radar data. It should be noted that some data preprocessing, such as orbital file correction, GRD boundary correction, thermal noise reduction, radiometric calibration, terrain correction, and foreshortening masking, was also applied to Sentinel-1 data by GEE developers.

The preprocessing of Sentinel-2 data included radiometric calibration and resampling, as well as cloud, snow, and shadow masking [55]. Additionally, median values were calculated for all four months of pixels for the Sentinel-2 images from January 2020 to January 2022. Considering the four-month extraction based on seasonal changes and obtaining the median across the Sentinel-2 observations helped in masking clouds, snow, and other unwanted pixels.

3.1.3. Feature Extraction

Different features were extracted from both Sentinel-1 and Sentinel-2 mosaic images. In the case of Sentinel-1, the VV and VH polarizations were considered, while in the case of Sentinel-2, three visible, one NIR, two SWIR bands, the normalized difference vegetation index (NDVI), and the normalized difference water index (NDWI) were considered. These features were selected because they have proved useful for wetland discrimination [56–58]. The relevant features were calculated using various formulas and band ratios within the GEE platform, separately for Sentinel-1 and Sentinel-2. Finally, two mosaic images containing 12 Sentinel-1 feature layers and 48 Sentinel-2 feature layers were produced to be used in the classification model.

3.2. Classification Model

As mentioned earlier, an object-based supervised classification algorithm was implemented in this study due to its higher accuracy and better quality in terms of visual perspective (e.g., fewer salt-and-pepper effects compared with pixel-based methods) [19,39,47,48,59]. The proposed method in this study can be divided into three distinct steps: image segmentation, first segment classification, and second classification. The novelty of this approach lies in the two-step classification process, which is explained in detail in the following sections. Each step plays a crucial role in achieving accurate and reliable wetland mapping results.

3.2.1. Segmentation

The first step of an object-based classification algorithm is segmentation, involving grouping homogeneous pixels into spectrally similar image segments. The primary objective of the segmentation process is to enhance the interpretability and classification of the image by transforming its characteristics into more meaningful representations. By utilizing image segments that better capture the objects within the landscape compared with individual pixels, each stage of the classification process, from defining training sites to classifying based on these segments, becomes more streamlined. Furthermore, this approach can lead to improved accuracy in classification outcomes. In this study, the

Simple Non-Iterative Clustering (SNIC) segmentation algorithm [60], available in GEE [61], was implemented. SLIC is a developed Simple Linear Iterative Clustering (SLIC) segmentation technique that was enhanced by removing the iterative process and enforcing the connectivity restrictions from the first step [33]. In the SNIC segmentation algorithm, a user-defined number of seed points were placed on a regular grid in image space, which were then grown using four-axis connectivity rules and a distance measure. In segments containing point-based samples, the segment labels were determined based on the class that had the highest number of points within that segment. All segments with labels were also separated randomly using GEE into two groups of training (70%) and testing (30%).

3.2.2. Classification

After segmentation, all segments must be classified. In this study, the RF classification method was utilized. The RF classifier is a non-parametric ML algorithm that consists of an ensemble of decision trees, each of which consists of several nodes to divide the input objects into mutually exclusive groups [23]. Previous studies have evaluated various ML classification methods, and most of them introduced RF as the most effective classification algorithm for wetland mapping [48,59,62].

In this study, we used the RF classification algorithm with a novel strategy to produce the wetland map. In the proposed method, training and applying the RF model were performed in two steps. The two-step RF classification model used in this study had two main objectives: (1) initial separation of classes that can be distinguished with much greater accuracy using optical, thermal, and radar RS measurements, and (2) avoiding systematic errors incurred by the unequal distribution of training samples across different classes. The underlying concept of this method was that the Open Water, Cropland, and Barren classes might be easily distinguished using elevation data and time-series optical and radar observations due to their distinctive spectral properties. In general, croplands are usually found in flat areas with slopes of less than 2% and have very high vegetation index values twice a year (usually spring and fall or both). Furthermore, water bodies, mountains, arid terrain, and urban areas are highly identifiable with radar data and optical observations due to their texture and spectral properties. On the other hand, the spectral properties of wetlands differ from those of the corresponding classes and are typically similar to both grasslands (for example bogs and grasslands) and forests (swamps and forests).

- Initial classification

First, an RF model was applied to all segments to classify them into four classes of Barren, Cropland, Open Water, and Other segments which were for wetland, Grassland/Shrubland, and Forest classes. To achieve this, the initial Random Forest (RF) model was trained using all available features, utilizing 70% of the training segments that belonged to the Barren, Cropland, Open Water, and Other classes. Subsequently, the trained RF model was tested using the remaining 30% of the segments that were labeled. If the accuracy of the trained RF model met the predetermined acceptable accuracy threshold for classification, the trained RF model was then applied to classify all segments within the study area. The output of this step was an initial map with four classes: Barren, Cropland, Open Water, and Other. This map was used as the input for the next step to create the final wetland map.

- Final classification

After generating the initial map, the segments classified as "Other" during the first classification were specifically selected for the subsequent RF model. In this step, these segments were further divided into four distinct wetland classes (Fen, Bog, Swamp, and Marsh), as well as the Forest and Grassland/Shrubland classes.

Four types of wetlands, including Bog, Fen, Marsh, and Swamp, were defined based on CWCS for wetland classification in GL. According to [7], CWCS differentiated these classes based on the soil properties, nutrition conditions, water sources, water table, hydrology, and vegetation characteristics. Bog is an ombrotrophic peatland with organic soil and

an acidic and oligotrophic nutrition environment. This class is dominated by bryophytes (sphagnum moss), graminoids (sedges), and ericaceous shrubs. On the other hand, Fen is a minerotrophic peatland, indicating precipitation, underground, and surface flows as water sources. Fen is mainly covered by Bryophytes (brown and sphagnum mosses), graminoids (sedges), and shrubs with organic soil and variant nutrient condition (such as Eutrophic, mesotrophic, and oligotrophic) which lead to rich and poor fens. Swamp is a minerogenous woody wetland dominated by woody vegetation, including trees and shrubs greater than 1 m and forbs. Swamps can have a higher degree of water level fluctuation compared with bogs and fens. Swamps on mineral or organic soils are considered the driest wetland type due to their lower water table and reduced water saturation levels. Marsh is a minerogenous wetland characterized by mineral soil and standing or flowing water with high water-level fluctuation from daily to annually. Aquatic emergent graminoids and shrubs are the dominant vegetation types that typically cover marshes.

To train the RF classifier during this step, the training samples originally belonging to the aforementioned classes, which had been labeled as "Other" during initial RF classification, were reclassified back into their original classes. These reclassified training samples were then utilized to train the RF classifier in order to accurately classify the segments into the specific wetland, Forest, and Grassland/Shrubland classes. Consequently, the output of this step was the final wetland map with nine classes.

3.3. Accuracy Assessment

To assess the accuracy of the proposed method and the resulting wetland map, we initially conducted a visual interpretation using high-resolution imagery available in ArcGIS. This step aimed to ensure the reliability of the final wetland map by comparing several random locations with various classes against the high-resolution images. This assessment helped us evaluate the level of agreement and identify any discrepancies or misclassifications. Furthermore, a statistical accuracy assessment was performed using an independent 30% of field samples to quantify the accuracy of the final wetland map. To accomplish this, we created a confusion matrix and utilized several metrics, including:

Overall Accuracy (OA)—This metric represents the proportion of correctly classified wetland pixels relative to the total number of pixels in the assessment dataset. OA provides a general measure of the classification accuracy.

Kappa coefficient (KC)—The KC is a statistical measure that evaluates the agreement between the predicted and actual wetland classes, considering the agreement that could be expected by chance. It considers the distribution of the observed and predicted classes and provides a more robust measure of classification accuracy than OA alone.

Producer Accuracy (PA)—PA refers to the proportion of correctly classified wetland pixels for each specific wetland class. It assesses how effectively the proposed method identifies a particular wetland class.

User Accuracy (UA)—UA represents the proportion of correctly classified wetland pixels for each predicted wetland class. It measures the reliability of the proposed method in assigning a specific wetland class.

4. Results

4.1. Classified Wetland Map

Figure 4 shows the final wetland map generated by the proposed object-based supervised classification algorithm in GEE at a spatial resolution of 10 m. Based on the results, the Open Water bodies of Superior, Michigan, Huron, Erie, and Ontario lakes represent a major part of the study area. The terrestrial portion of the study area is mostly covered by woodland and forest in the north and a large portion of croplands in the south and southeast regions. Additionally, the distribution of the Barren class is more visible in the southern regions.

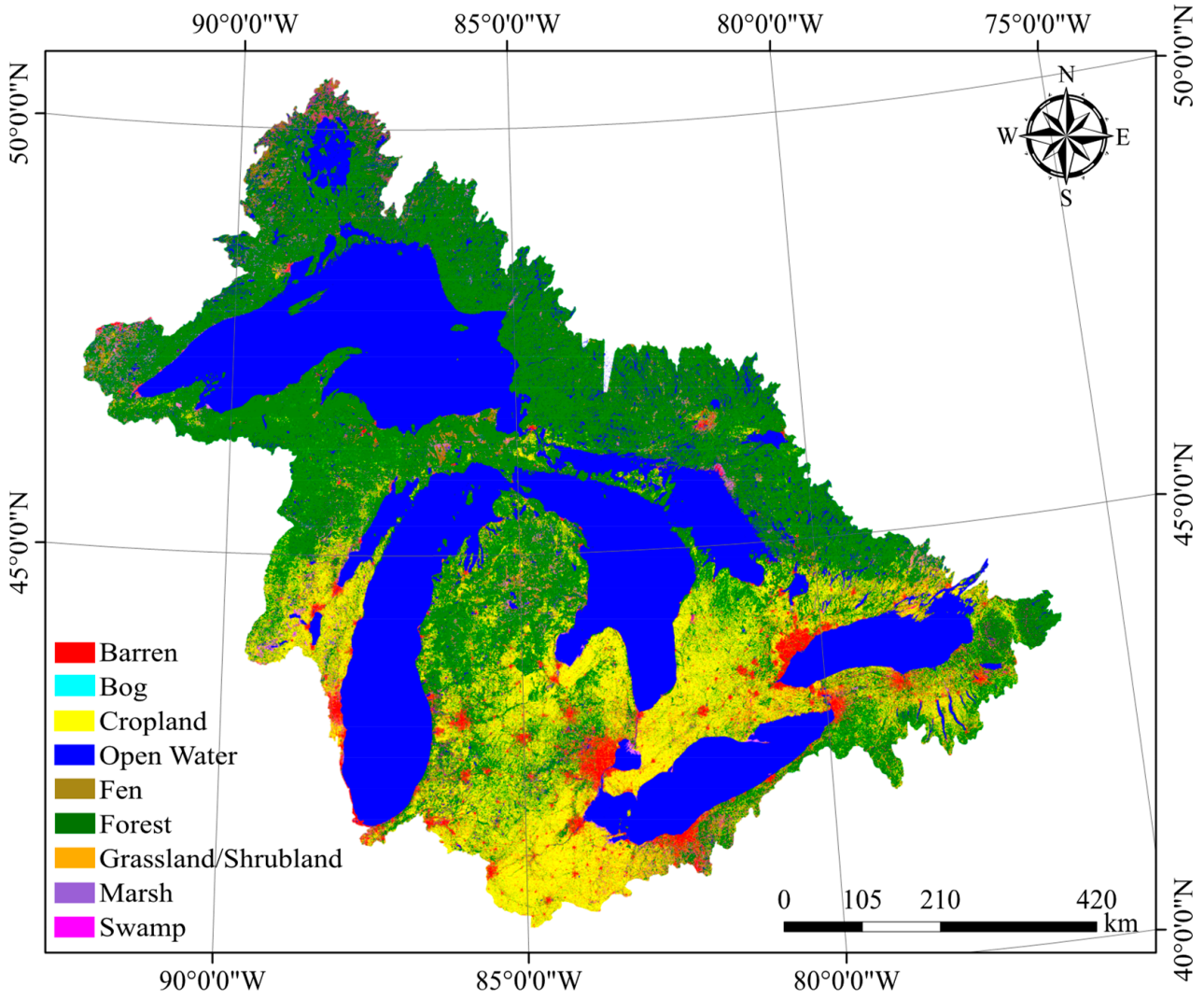

Figure 4. GL wetland map.

Eight zoomed areas from the final wetland map are also illustrated in Figure 5 to show the visual accuracy of the produced wetland map. The results of the visual investigation demonstrated the high potential of the proposed method within GEE to identify various wetland classes in regions like the GL with diverse climate conditions (Figure 5a,g,h). Moreover, the proposed methodology correctly identified non-wetland classes, such as urban areas. Notably, despite the high similarity between forests and croplands, the proposed approach accurately differentiated between them (Figure 5a–d). The classification method also effectively distinguished Marsh from Croplands, although there were occasional challenges in visually differentiating them in certain areas (Figure 5a,b). However, there were instances where certain classes were misclassified as Marsh (Figure 5b,f). This misclassification can be attributed to the intrinsic complexity and variability of the land cover patterns in those specific areas, making it challenging to accurately distinguish Marsh from other land cover classes. Overall, based on Figure 5, there were complex land covers in some areas which were challenging to identify. For example, swamps (tree wetlands), which were distributed all over the study area, were difficult to identify from aerial or satellite imagery, and in many cases, they were visually confused with forests (Figure 5d,e).

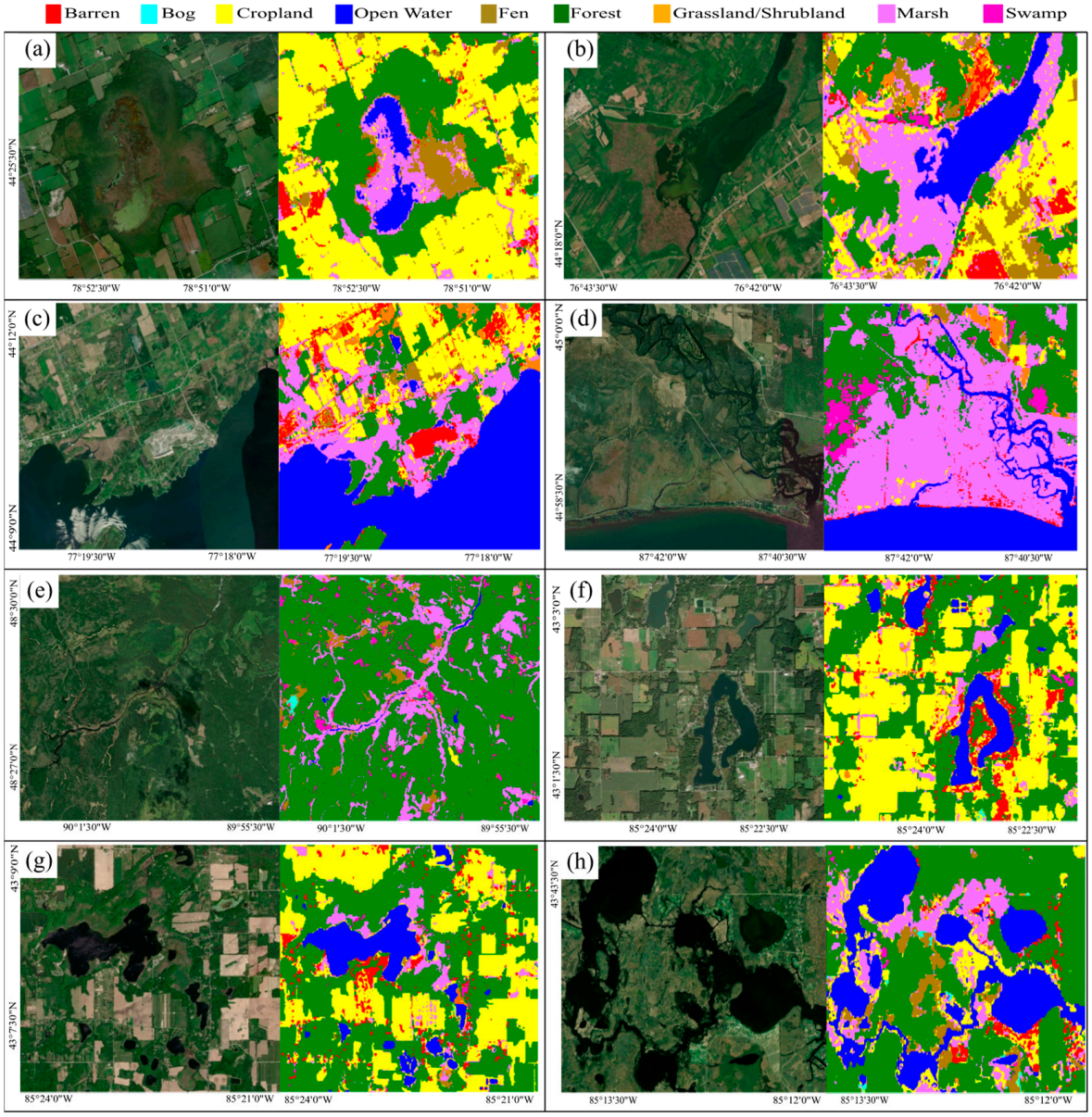

Figure 5. Eight zoomed areas from the final wetland map along with their corresponding high-resolution images. (**a**–**h**) Each subfigure represents a different combination of wetland and non-wetland land cover that exists in the study area.

4.2. Distribution of the Wetland Classes in the GL

Figure 6 shows the distribution of different classes in five sub-basins of the GL. Based on the results, Open Water and Forest are the dominant classes across all sub-basins except Erie. For example, these two classes account for 89% and 66% of the Superior and Michigan sub-basins. Across both of these sub-basins, Open Water is the dominant class, which covers 45% of Superior and 35% of Michigan. In the Ontario and Huron sub-basins, the Forest class is dominant, with coverages of 34% and 39%, respectively. In Erie, Cropland with a coverage of 47% is the dominant class, followed by Open Water with 26% coverage. Cropland also covers 26%, 23%, and 17% of the Ontario, Michigan, and Huron sub-basins. Finally, the results showed that Cropland, Barren, and Grassland/Shrubland are rarely found in the Superior sub-basin, and Grassland/Shrubland also covers equal to or less than 2% of the other sub-basins.

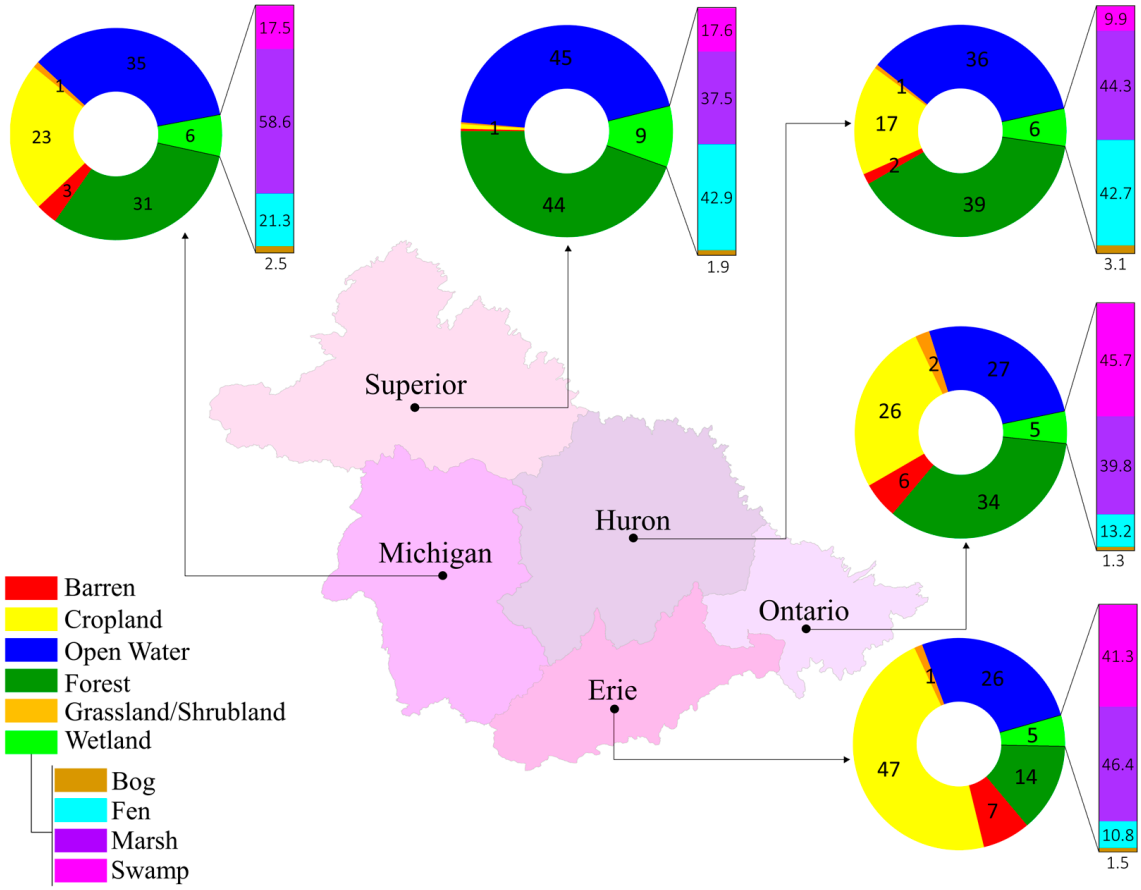

Figure 6. Distribution of wetland and non-wetland classes in five sub-basins of GL.

Based on Figure 6, wetlands (i.e., Bog, Fen, Marsh, and Swamp) contain less than 10% of all sub-basins. Superior has the most wetland coverage (~9%) compared with other sub-basins. In Superior, Fen, with 42.9%, is the most dominant wetland class, followed by Marsh (37.5%) and Swamp (17.6%). In the Huron and Michigan sub-basins, Marsh is the dominant wetland class, followed by Fen and Swamp. Swamp, with a coverage of 45.7% of wetland areas, is the most observed type of wetland in Ontario. After Swamp, Marsh, with 39.8%, and Fen, with 13.2%, of wetland coverage are found as the main wetland species in Ontario. Moreover, Marsh, with a coverage of 46.4%, and Swamp, with a coverage of 41.3%, are the most dominant wetlands in Erie. The Bog class has the least coverage in all the sub-basins. Overall, Bog has an average coverage of 2% of the total wetland areas.

4.3. Statistical Accuracy Assessment

Table 3 provides the confusion matrix of the proposed method using the independent test data. Nine LULC classes' UAs and PAs are also included in Table 3. According to Table 3, the PAs and UAs of the nine classes ranged between 55.45–99.64% and 30.29–98.62%, respectively. Based on the PAs, the Open Water and Forest classes were classified with the highest accuracies (i.e., PAs were 99.64% and 98.16%, respectively). Moreover, Barren, Cropland, and Fen were classified with PAs of more than 90%. Grassland/Shrubland, with a PA of 55.45%, had the lowest PA. This was mainly because there were many Grassland/Shrubland reference samples that were wrongly classified as Cropland (494 samples) and Forest (215 samples). Regarding the UAs, all classes, except Forest, Grassland/Shrubland, and Barren, were classified with accuracies of more than 90%. Bog, with a UA of 98.62; Swamp, with a UA of 97.98; and Open Water, with a UA of 97.01, were classified with the highest UAs. However, similar to the results of the PAs, Grassland/Shrubland, with a UA of 30.29%, had the lowest UA. The main reason was the

fact that there were many Marsh samples (1826 samples) that were incorrectly classified as Grassland/Shrubland. Thus, there was an overestimation in the classified areas of Grassland/Shrubland in the produced wetland map.

Table 3. The confusion matrix of the wetland map of the GL, along with UAs and PAs of each class.

		Predicted Samples									
		Barren	Bog	Cropland	Open Water	Fen	Forest	Grassland/ Shrubland	Marsh	Swamp	PA
Reference Samples	Barren	21,784	1	1193	90	69	67	213	455	5	91.23%
	Bog	1	1862	335	5	41	257	0	34	3	73.36%
	Cropland	2218	15	217,888	79	1027	5985	483	483	94	95.45%
	Open Water	23	0	140	56,495	1	14	0	24	3	99.64%
	Fen	26	1	323	5	13,878	212	2	29	4	95.84%
	Forest	46	3	587	17	29	45,488	9	50	114	98.16%
	Grassland/ Shrubland	90	0	494	3	4	215	1104	60	21	55.45%
	Marsh	252	6	3855	1535	71	488	1826	15,827	44	66.21%
	Swamp	845	0	673	5	30	1113	8	29	13,999	83.82%
	UA	86.15%	98.62%	96.63%	97.01%	91.60%	84.49%	30.29%	93.15%	97.98%	

Figure 7 summarizes the OA, KC, Average PA (APA), and Average UA (AUA) for the wetland and non-wetland classes. Based on Figure 7, the classification algorithm obtained an OA, KC, APA, and AUA of 87%, 0.91, 79.81%, and 95.34% for wetland classes, respectively. Overall, the results also showed that the non-wetland classes were identified more accurately than the wetland classes. For instance, the OA, KC, APA, and AUA for non-wetland classes were 96.62%, 0.95, 87.98%, and 78.91%, respectively.

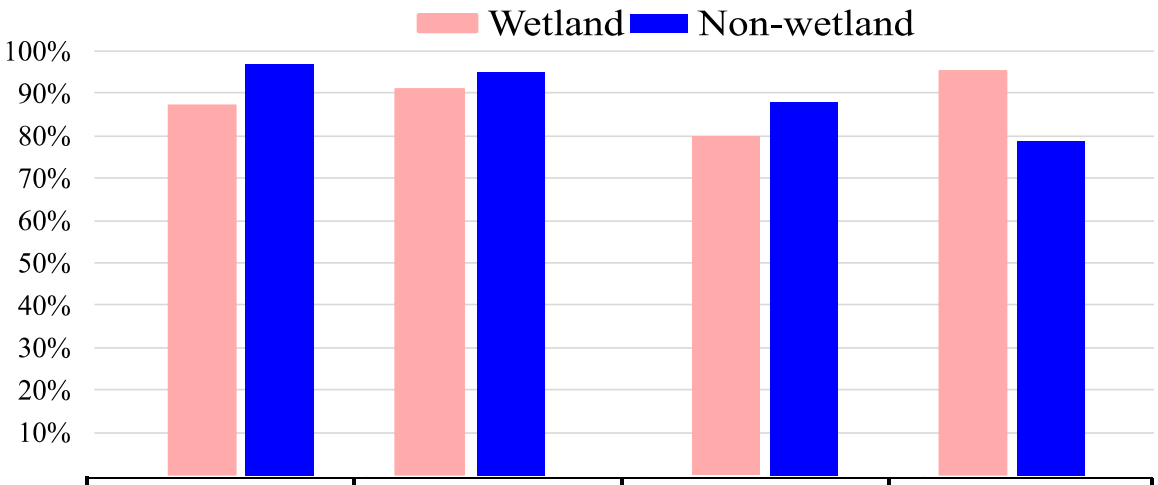

	OA	KC	APA	AUA
Wetland	87.00%	0.91	79.81%	95.34%
Non-wetland	96.62%	0.95	87.98%	78.91%

Figure 7. Overall accuracy (OA), Kappa coefficient (KC), Average PA (APA), and Average UA (AUA) of the proposed method for wetland and non-wetland classes.

Figure 8 provides the accuracies of all classes for each sub-basin of the GL. In all sub-basins, the OAs were more than 90%. The highest and lowest OAs of the final classified wetland map were over Huron (OA = 97.8%) and Ontario (OA = 90.6%). Moreover, Erie and Michigan had the highest (KC = 0.94) and lowest (KC = 0.84) KC values. The details of

the statistical metrics of each of the nine considered classes of all five sub-basins are also provided in Tables A1–A5 and Figure A1 in the Appendix A.

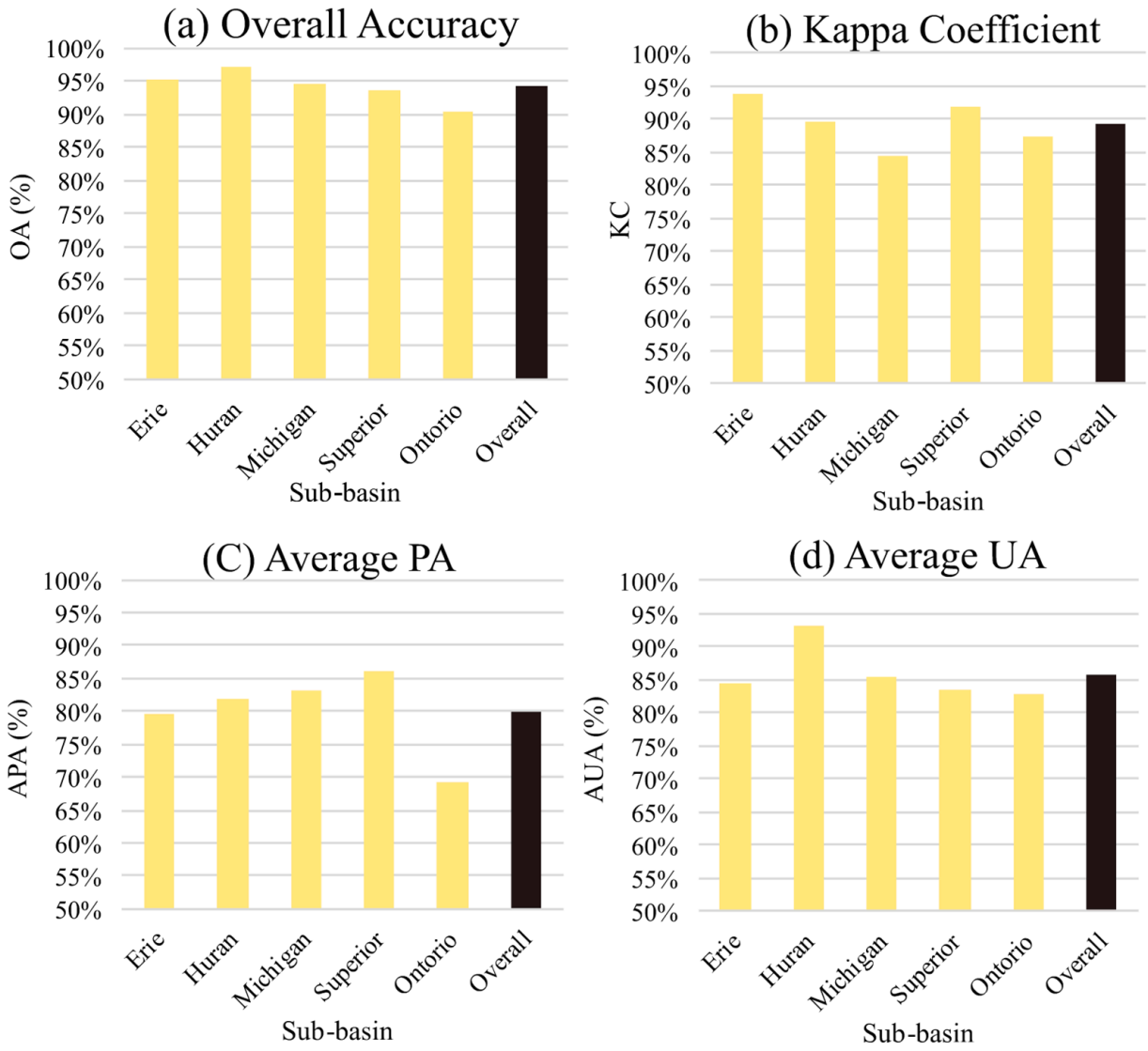

Figure 8. The (**a**) overall accuracy (OA), (**b**) Kappa coefficient (KC), (**c**) Average Producer Accuracy (APA), and (**d**) Average User Accuracy (AUA) of the classified wetland map for each sub-basin of the GL.

5. Discussion

Applying the proposed ML classification method or alternative classification methods to identify and map different wetland types can present certain challenges within the GEE environment. These challenges may arise from factors such as in situ data availability, RS data quality, the characteristics of the study area, and the diversity of wetland types.

In this study, we took a comprehensive approach by utilizing extensive in situ wetland samples collected by various organizations in Canada. This allowed us to enhance the accuracy and reliability of our wetland classification results. However, the distribution and number of samples of different wetland classes can cause some errors for wetland classification using RS techniques. For example, according to the areas of different classes in the produced wetland map of the GL (Figure 4), Forest (46.85%), followed by Open Water (26.30%) and Cropland (10.49%), are the most dominant land covers in the study area. Moreover, each of the Bog, Marsh, Fen, and Swamp classes only covers less than 10%

of the study area. However, according to Table 2, out of 3215 in situ samples, 1080 (33% of the samples) belong to the Marsh class, and only 555 (17%) and 83 (2%) belong to the Forest and Barren classes, respectively. The asymmetry between the coverage and the number of in situ samples of each class resulted in classification errors [63,64]. This issue can pose a significant challenge when applying the proposed method to map wetlands of the area with fewer in situ samples. In general, to effectively implement supervised classification, an adequate number of samples that accurately represent the various types of land cover, considering both the sample quantity and the coverage area, is crucial.

Moreover, acquiring representative samples of wetlands can be particularly challenging due to their spatial extent and ecological complexity. Wetlands encompass a wide range of ecosystems, including marshes, swamps, bogs, and floodplains, each with distinct vegetation, hydrological patterns, and soil compositions [7,26,65,66]. Therefore, to achieve reliable wetland mapping, it is crucial to ensure that the collected samples capture the full range of variability within wetland ecosystems.

Furthermore, the size of the study area also plays a critical role in determining the number of required samples. Larger study areas with extensive wetland coverage demand a more comprehensive sampling strategy to ensure adequate representation of the different wetland types present. Insufficient samples within such areas can result in biased classification results and limited applicability of the proposed method.

Moreover, the spectral and backscattering responses of different wetland ecosystems can be similar to each other and other non-wetland classes. This was the main reason for the confusion between several classes in the classified map (Table 3). For example, there were many Barren samples that were wrongly classified as Cropland (i.e., 1193 samples). This can be explained by the fact that many croplands were cultivated and, therefore, were similar to Barren in the satellite imagery. As another example, the Marsh class was confused with either Cropland, Grassland/Shrubland, or Open Water, where many Marsh samples were wrongly classified as these three classes (i.e., 3855, 1826, and, 1535, respectively). These misclassifications could be explained by the seasonal changes in these classes. For example, during spring, most Marsh areas are inundated and, thus, some of them can have a similar spectral response to Open Water. This shows the importance of multi-temporal satellite images for distinguishing wetland classes.

GEE offers an extensive collection of geospatial datasets accompanied by a diverse range of image processing and ML algorithms. The availability of numerous satellite images, including those that have been atmospherically and noise-corrected, in conjunction with a coding workspace and a wide array of toolboxes and ML algorithms, greatly facilitates continental- and global-scale wetland mapping studies. The comprehensive capabilities provided by GEE significantly reduce the necessity for multiple software packages dedicated to data reading, processing, and coding. As a result, GEE emerges as an invaluable resource for researchers conducting large-scale wetland mapping endeavors. However, GEE has several limitations which hinder obtaining the highest possible classification accuracy. For example, implementing an ML model in GEE is restricted to a limited number of training samples and, therefore, it was not possible to increase the number of samples to improve the classification accuracy. One solution might be employing other cloud computing platforms, such as Amazon's Web Services and Microsoft's Azure in future studies.

GEE has recently enhanced its platform to deploy DL classification techniques in addition to current ensemble ML algorithms. Although RF has resulted in a high classification accuracy in many studies, DL models demonstrated better accuracies in recent studies [67–70]. Consequently, it is suggested to implement object-based DL classification algorithms to possibly obtain better accuracies.

The proposed wetland classification method can effectively be applied to produce yearly and seasonal wetland maps in the GL. Therefore, it is suggested to use the proposed GEE method to generate wetland change maps at a 10 m spatial resolution from 2016 to the present. This wetland change analysis would provide crucial information about

deforestation, urbanization, and crop expansion and, consequently, would improve better wetland management in the GL.

6. Conclusions

Wetlands are threatened by agricultural activities, construction work, population increase, and natural processes, such as global warming, changing precipitation patterns, and coastal erosion. Therefore, it is necessary to produce accurate wetland maps. In this study, the most recent wetland map of the GL, including Fen, Swamp, Marsh, and Bog, was produced in GEE. To this end, a novel two-step object-based supervised RF classification algorithm was implemented using Sentinel-1 backscattering data, Sentinel-2 multispectral imagery, and DEM data. In the first step, all image segments were divided into four classes of Barren, Cropland, Open Water, and Other. In the second step, the Barren, Cropland, and Open Water segments were excluded from the classification, and the remaining segments were divided into six classes of Forest, Grassland/Shrubland, Fen, Bog, Swamp, and Marsh.

The combination of Sentinel-1/2 imagery and DEM data in GEE offers powerful synergies for diverse applications. Integrating radar and optical data enables comprehensive surface understanding, enhancing land cover classification, change detection, and vegetation monitoring. Incorporating DEM data enables terrain analysis, feature extraction, and flood mapping. These datasets, easily accessible in GEE, empower efficient analysis and provide valuable insights for various applications.

The accuracy of the GL wetland map was investigated from different perspectives. The proposed method was able to classify the wetland classes with an OA, KC, APA, and AUA of 87%, 0.91, 79.81%, and 95.34%, respectively. The results also demonstrated that non-wetland classes were identified more accurately (OA = 96.62%, KC = 0.9498, APA = 87.98%, and AUA = 78.91%). More details about the accuracy of each class all over the study area, the accuracy of the wetland map over each sub-basin, the accuracy of every class in each sub-basin, and the distribution of LULC classes in five sub-basins were also reported in this study. The results of this study showed that GEE was a very powerful platform for large-scale wetland mapping and monitoring tasks. Additionally, the proposed method can effectively be applied to study wetland changes in the future.

Author Contributions: Conceptualization, M.A., F.M. and M.K.; methodology, M.K. and M.A.; software, M.K., M.A. and F.M.; validation, F.M., M.A., P.M. and M.K.; formal analysis, F.M.; investigation, F.M., M.A., P.M. and M.K.; resources, M.A.; data curation, F.M., M.K., P.M. and M.A.; writing—original draft preparation, F.M. and M.A.; writing—review and editing, F.M., M.A., P.M., A.M. and M.K.; visualization, F.M.; supervision, M.A. and S.J. All authors have read and agreed to the published version of the manuscript.

Funding: This research received no external funding.

Data Availability Statement: All satellite data and products supporting the methodology and findings of this paper (including Sentinel-1 corrected backscattering data, Sentinel-2 reflectance images, and SRTM-DEM) have been archived in GEE and are openly available at https://developers.google.com/earth-engine/datasets/catalog/, accessed on 6 July 2023. The field samples of wetland and non-wetland classes over different GL basins, which were used in this study to train and validate the proposed classification method, were collected using the GEE cloud computing platform at https://code.earthengine.google.com/, accessed on 6 July 2023.

Conflicts of Interest: The authors declare no conflict of interest.

Appendix A

Table A1. The confusion matrix of the LULC map over Erie, along with UAs and PAs of nine LULC classes. Erie, OA = 95.65%, Average PA = 84.38%, Average UA = 80.35, KC = 0.9384.

		MAP									
	Erie	Barren	Bog	Cropland	Open Water	Fen	Forest	Grassland/ Shrubland	Marsh	Swamp	PA
In situ	Barren	5063	0	28	0	1	21	108	7	0	96.84%
	Bog	0	0	0	0	0	0	0	0	0	0
	Cropland	260	2	29,263	1	21	277	356	51	16	96.75%
	Open Water	20	0	21	6860	0	2	0	1	1	99.35%
	Fen	15	0	1	0	11	9	0	0	0	30.56%
	Forest	12	0	13	0	1	6047	1	3	43	98.81%
	Grassland/ Shrubland	17	0	81	0	1	54	501	1	27	73.46%
	Marsh	139	1	406	35	21	137	41	4696	19	85.46%
	Swamp	78	0	41	0	0	231	6	7	5585	93.90%
	UA	90.35%	0	98.02%	99.48%	19.64%	89.22%	49.46%	98.53%	98.14%	

Table A2. The confusion matrix of the LULC map over Michigan, along with UAs and PAs of nine LULC classes. Michigan, OA = 87.20%, Average PA = 85.16%, Average UA = 74.56%, KC = 0.844.

		MAP									
	Michigan	Barren	Bog	Cropland	Open Water	Fen	Forest	Grassland/ Shrubland	Marsh	Swamp	PA
In situ	Barren	3154	0	66	0	9	20	68	18	7	94.37%
	Bog	0	703	131	1	6	84	0	15	1	74.71%
	Cropland	19	3	2899	1	0	410	0	1	0	86.98%
	Open Water	6	0	78	392	0	4	0	2	0	81.33%
	Fen	3	0	283	1	1863	45	0	10	0	84.49%
	Forest	4	0	6	0	2	1980	2	6	4	98.80%
	Grassland/ Shrubland	0	0	0	0	0	0	69	0	0	
	Marsh	47	0	339	123	9	39	0	1714	1	75.44%
	Swamp	0	0	0	0	0	0	0	0	0	
	UA	97.56%	99.58%	76.25%	75.68%	98.62%	76.68%	49.64%	97.06%	0.00%	

Table A3. The confusion matrix of the LULC map over Superior, along with UAs and PAs of nine LULC classes. Superior, OA = 93.75%, Average PA = 86.84%, Average UA = 83.59%, KC = 0.918.

		MAP									
	Superior	Barren	Bog	Cropland	Open Water	Fen	Forest	Grassland/ Shrubland	Marsh	Swamp	PA
In situ	Barren	1953	2	180	4	55	19	26	439	0	72.93%
	Bog	0	872	0	1	22	76	0	3	2	89.34%
	Cropland	1	0	935	0	32	0	295	1	0	73.97%
	Open Water	0	0	0	3164	0	0	0	3	0	99.91%
	Fen	0	0	0	0	9486	115	0	10	1	98.69%
	Forest	2	2	1	5	18	9021	0	12	22	99.32%
	Grassland/ Shrubland	0	0	0	0	0	11	53	0	0	82.81%
	Marsh	0	4	0	33	9	70	0	998	1	89.51%
	Swamp	1	0	2	4	29	308	1	13	1082	75.14%
	UA	99.80%	99.09%	83.63%	98.54%	98.29%	93.77%	14.13%	67.48%	97.65%	

Table A4. The confusion matrix of the LULC map over Huron, along with UAs and PAs of nine LULC classes. Huron, OA = 94.51%, Average PA = 83.09%, Average UA = 85.56%, KC = 0.897.

		MAP									
	Huron	Barren	Bog	Cropland	Open Water	Fen	Forest	Grassland/ Shrubland	Marsh	Swamp	PA
In situ	Barren	6228	0	34	74	4	0	0	1	0	98.22%
	Bog	1	286	204	3	12	99	0	15	0	46.13%
	Cropland	2074	14	149,127	77	988	5413	140	429	70	94.19%
	Open Water	0	0	0	40,522	1	5	0	0	0	99.99%
	Fen	2	1	9	4	2393	28	0	3	1	98.03%
	Forest	19	1	20	10	8	17,275	2	11	39	99.37%
	Grassland/ Shrubland	3	0	97	2	3	143	529	43	1	64.43%
	Marsh	65	0	702	1302	30	191	4	4141	22	64.13%
	Swamp	2	0	33	0	1	496	0	1	2675	83.39%
	UA	74.20%	94.70%	99.27%	96.49%	69.56%	73.04%	78.37%	89.17%	95.26%	

Table A5. The confusion matrix of the LULC map over Ontario, along with UAs and PAs of nine LULC classes. Ontario, OA = 91%, Average PA = 73.28%, Average UA = 74.66%, KC = 0.872.

		MAP									
	Ontario	Barren	Bog	Cropland	Open Water	Fen	Forest	Grassland/ Shrubland	Marsh	Swamp	PA
In situ	Barren	5951	0	305	13	0	14	30	0	0	94.27%
	Bog	0	0	0	0	0	1	0	0	0	0.00%
	Cropland	262	3	32,514	5	46	2040	181	84	16	92.50%
	Open Water	0	0	0	5617	0	0	1	15	0	99.72%
	Fen	6	0	0	0	155	16	2	7	3	82.01%
	Forest	14	0	17	0	2	11,762	8	6	5	99.56%
	Grassland/ Shrubland	122	0	88	0	1	25	169	18	1	39.86%
	Marsh	18	0	1923	46	1	39	20	4748	1	69.86%
	Swamp	800	0	228	0	0	78	2	4	4994	81.79%
	UA	82.96%	0.00%	92.70%	98.87%	75.61%	84.16%	40.92%	97.26%	99.48%	

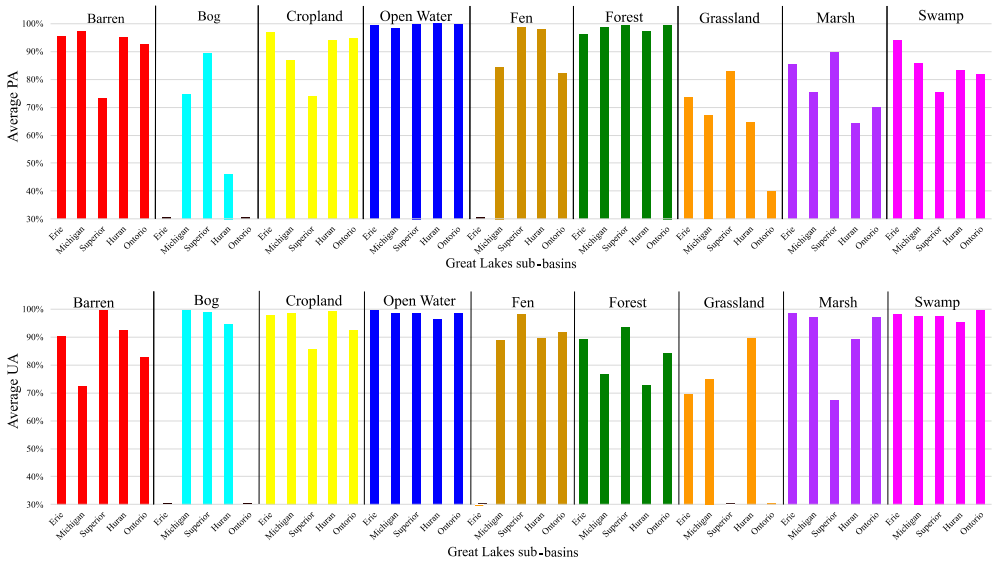

Figure A1. The accuracy report of each of the nine LULC classes, separately for each sub-basin.

References

1. Yang, Z.; Bai, J.; Zhang, W. Mapping and assessment of wetland conditions by using remote sensing images and POI data. *Ecol. Indic.* **2021**, *127*, 107485. [CrossRef]
2. Jha, C.S.; Dutt, C.B.; Bawa, K.S. Deforestation and land use changes in Western Ghats, India. *Curr. Sci.* **2000**, *79*, 231–238.
3. Kayet, N.; Pathak, K.; Chakrabarty, A.; Sahoo, S. Spatial impact of land use/land cover change on surface temperature distribution in Saranda Forest, Jharkhand. *Model. Earth Syst. Environ.* **2016**, *2*, 127. [CrossRef]
4. Dorren, L.K.; Maier, B.; Seijmonsbergen, A.C. Improved Landsat-based forest mapping in steep mountainous terrain using object-based classification. *For. Ecol. Manag.* **2003**, *183*, 31–46. [CrossRef]
5. Stević, D.; Hut, I.; Dojčinović, N.; Joković, J. Automated identification of land cover type using multispectral satellite images. *Energy Build.* **2016**, *115*, 131–137. [CrossRef]
6. Gavade, A.B.; Rajpurohit, V.S. Systematic analysis of satellite image-based land cover classification techniques: Literature review and challenges. *Int. J. Comput. Appl.* **2021**, *43*, 514–523. [CrossRef]
7. Mahdavi, S.; Salehi, B.; Granger, J.; Amani, M.; Brisco, B.; Huang, W. Remote sensing for wetland classification: A comprehensive review. *GIScience Remote Sens.* **2018**, *55*, 623–658. [CrossRef]
8. Mirmazloumi, S.M.; Moghimi, A.; Ranjgar, B.; Mohseni, F.; Ghorbanian, A.; Ahmadi, S.A.; Amani, M.; Brisco, B. Status and trends of wetland studies in Canada using remote sensing technology with a focus on wetland classification: A bibliographic analysis. *Remote Sens.* **2021**, *13*, 4025. [CrossRef]
9. Amani, M.; Kakooei, M.; Ghorbanian, A.; Warren, R.; Mahdavi, S.; Brisco, B.; Moghimi, A.; Bourgeau-Chavez, L.; Toure, S.; Paudel, A.; et al. Forty years of wetland status and trends analyses in the Great Lakes using Landsat archive imagery and Google Earth Engine. *Remote Sens.* **2022**, *14*, 3778. [CrossRef]
10. Gao, Y.; Mas, J.F. A comparison of the performance of pixel-based and object-based classifications over images with various spatial resolutions. *Online J. Earth Sci.* **2008**, *2*, 27–35.
11. Guo, R.; Liu, J.; Li, N.; Liu, S.; Chen, F.; Cheng, B.; Duan, J.; Li, X.; Ma, C. Pixel-wise classification method for high resolution remote sensing imagery using deep neural networks. *ISPRS Int. J. Geo-Inf.* **2018**, *7*, 110. [CrossRef]
12. Duro, D.C.; Franklin, S.E.; Dubé, M.G. A comparison of pixel-based and object-based image analysis with selected machine learning algorithms for the classification of agricultural landscapes using SPOT-5 HRG imagery. *Remote Sens. Environ.* **2012**, *118*, 259–272. [CrossRef]
13. Li, M.; Zang, S.; Zhang, B.; Li, S.; Wu, C. A review of remote sensing image classification techniques: The role of spatio-contextual information. *Eur. J. Remote Sens.* **2014**, *47*, 389–411. [CrossRef]
14. Qu, L.A.; Chen, Z.; Li, M.; Zhi, J.; Wang, H. Accuracy improvements to pixel-based and object-based lulc classification with auxiliary datasets from Google Earth engine. *Remote Sens.* **2021**, *13*, 453. [CrossRef]
15. Pan, X.; Zhang, C.; Xu, J.; Zhao, J. Simplified object-based deep neural network for very high resolution remote sensing image classification. *ISPRS J. Photogramm. Remote Sens.* **2021**, *181*, 218–237. [CrossRef]
16. Tian, Y.; Yang, C.; Huang, W.; Tang, J.; Li, X.; Zhang, Q. Machine learning-based crop recognition from aerial remote sensing imagery. *Front. Earth Sci.* **2021**, *15*, 54–69. [CrossRef]
17. Berhane, T.M.; Lane, C.R.; Wu, Q.; Anenkhonov, O.A.; Chepinoga, V.V.; Autrey, B.C.; Liu, H. Comparing pixel-and object-based approaches in effectively classifying wetland-dominated landscapes. *Remote Sens.* **2017**, *10*, 46. [CrossRef]
18. Liu, H.; Jiang, Q.; Ma, Y.; Yang, Q.; Shi, P.; Zhang, S.; Tan, Y.; Xi, J.; Zhang, Y.; Liu, B.; et al. Object-based multigrained cascade forest method for wetland classification using sentinel-2 and radarsat-2 imagery. *Water* **2022**, *14*, 82. [CrossRef]
19. Fatemighomi, H.S.; Golalizadeh, M.; Amani, M. Object-based hyperspectral image classification using a new latent block model based on hidden Markov random fields. *Pattern Anal. Appl.* **2022**, *25*, 467–481. [CrossRef]
20. Lu, D.; Weng, Q. A survey of image classification methods and techniques for improving classification performance. *Int. J. Remote Sens.* **2007**, *28*, 823–870. [CrossRef]
21. Richards, J.A.; Richards, J.A. Supervised classification techniques. In *Remote Sensing Digital Image Analysis*; Springer: Berlin/Heidelberg, Germany, 2022; pp. 263–367.
22. Maxwell, A.E.; Warner, T.A.; Fang, F. Implementation of machine-learning classification in remote sensing: An applied review. *Int. J. Remote Sens.* **2018**, *39*, 2784–2817. [CrossRef]
23. Talukdar, S.; Singha, P.; Mahato, S.; Pal, S.; Liou, Y.A.; Rahman, A. Land-use land-cover classification by machine learning classifiers for satellite observations—A review. *Remote Sens.* **2020**, *12*, 1135. [CrossRef]
24. Delalay, M.; Tiwari, V.; Ziegler, A.D.; Gopal, V.; Passy, P. Land-use and land-cover classification using Sentinel-2 data and machine-learning algorithms: Operational method and its implementation for a mountainous area of Nepal. *J. Appl. Remote Sens.* **2019**, *13*, 014530. [CrossRef]
25. Tu, Y.; Lang, W.; Yu, L.; Li, Y.; Jiang, J.; Qin, Y.; Wu, J.; Chen, T.; Xu, B. Improved mapping results of 10 m resolution land cover classification in Guangdong, China using multisource remote sensing data with Google Earth Engine. *IEEE J. Sel. Top. Appl. Earth Obs. Remote Sens.* **2020**, *13*, 5384–5397. [CrossRef]
26. Amani, M.; Mahdavi, S.; Afshar, M.; Brisco, B.; Huang, W.; Mohammad Javad Mirzadeh, S.; White, L.; Banks, S.; Montgomery, J.; Hopkinson, C. Canadian wetland inventory using Google Earth Engine: The first map and preliminary results. *Remote Sens.* **2019**, *11*, 842. [CrossRef]

27. Amani, M.; Brisco, B.; Afshar, M.; Mirmazloumi, S.M.; Mahdavi, S.; Mirzadeh, S.M.; Huang, W.; Granger, J. A generalized supervised classification scheme to produce provincial wetland inventory maps: An application of Google Earth Engine for big geo data processing. *Big Earth Data* **2019**, *3*, 378–394. [CrossRef]
28. Amani, M.; Mahdavi, S.; Kakooei, M.; Ghorbanian, A.; Brisco, B.; DeLancey, E.R.; Toure, S.; Reyes, E.L. Wetland change analysis in Alberta, Canada using four decades of landsat imagery. *IEEE J. Sel. Top. Appl. Earth Obs. Remote Sens.* **2021**, *14*, 10314–10335. [CrossRef]
29. Gorelick, N.; Hancher, M.; Dixon, M.; Ilyushchenko, S.; Thau, D.; Moore, R. Google Earth Engine: Planetary-scale geospatial analysis for everyone. *Remote Sens. Environ.* **2017**, *202*, 18–27. [CrossRef]
30. Amani, M.; Ghorbanian, A.; Ahmadi, S.A.; Kakooei, M.; Moghimi, A.; Mirmazloumi, S.M.; Moghaddam, S.H.; Mahdavi, S.; Ghahremanloo, M.; Parsian, S.; et al. Google earth engine cloud computing platform for remote sensing big data applications: A comprehensive review. *IEEE J. Sel. Top. Appl. Earth Obs. Remote Sens.* **2020**, *13*, 5326–5350. [CrossRef]
31. Kumar, L.; Mutanga, O. Google Earth Engine applications since inception: Usage, trends, and potential. *Remote Sens.* **2018**, *10*, 1509. [CrossRef]
32. Tamiminia, H.; Salehi, B.; Mahdianpari, M.; Quackenbush, L.; Adeli, S.; Brisco, B. Google Earth Engine for geo-big data applications: A meta-analysis and systematic review. *ISPRS J. Photogramm. Remote Sens.* **2020**, *164*, 152–170. [CrossRef]
33. Mirmazloumi, S.M.; Kakooei, M.; Mohseni, F.; Ghorbanian, A.; Amani, M.; Crosetto, M.; Monserrat, O. ELULC-10, a 10 m European land use and land cover map using sentinel and landsat data in google earth engine. *Remote Sens.* **2022**, *14*, 3041. [CrossRef]
34. Hird, J.N.; DeLancey, E.R.; McDermid, G.J.; Kariyeva, J. Google Earth Engine, open-access satellite data, and machine learning in support of large-area probabilistic wetland mapping. *Remote Sens.* **2017**, *9*, 1315. [CrossRef]
35. McCarthy, M.J.; Radabaugh, K.R.; Moyer, R.P.; Muller-Karger, F.E. Enabling efficient, large-scale high-spatial resolution wetland mapping using satellites. *Remote Sens. Environ.* **2018**, *208*, 189–201. [CrossRef]
36. Wang, X.; Xiao, X.; Zou, Z.; Hou, L.; Qin, Y.; Dong, J.; Doughty, R.B.; Chen, B.; Zhang, X.; Chen, Y.; et al. Mapping coastal wetlands of China using time series Landsat images in 2018 and Google Earth Engine. *ISPRS J. Photogramm. Remote Sens.* **2020**, *163*, 312–326. [CrossRef]
37. Mahdianpari, M.; Salehi, B.; Mohammadimanesh, F.; Brisco, B.; Homayouni, S.; Gill, E.; DeLancey, E.R.; Bourgeau-Chavez, L. Big data for a big country: The first generation of Canadian wetland inventory map at a spatial resolution of 10-m using Sentinel-1 and Sentinel-2 data on the Google Earth Engine cloud computing platform. *Can. J. Remote Sens.* **2020**, *46*, 15–33. [CrossRef]
38. Ghorbanian, A.; Zaghian, S.; Asiyabi, R.M.; Amani, M.; Mohammadzadeh, A.; Jamali, S. Mangrove ecosystem mapping using Sentinel-1 and Sentinel-2 satellite images and random forest algorithm in Google Earth Engine. *Remote Sens.* **2021**, *13*, 2565. [CrossRef]
39. Fekri, E.; Latifi, H.; Amani, M.; Zobeidinezhad, A. A training sample migration method for wetland mapping and monitoring using sentinel data in google earth engine. *Remote Sens.* **2021**, *13*, 4169. [CrossRef]
40. DeLancey, E.R.; Czekajlo, A.; Boychuk, L.; Gregory, F.; Amani, M.; Brisco, B.; Kariyeva, J.; Hird, J.N. Creating a Detailed Wetland Inventory with Sentinel-2 Time-Series Data and Google Earth Engine in the Prairie Pothole Region of Canada. *Remote Sens.* **2022**, *14*, 3401. [CrossRef]
41. White, L.; Ryerson, R.A.; Pasher, J.; Duffe, J. State of science assessment of remote sensing of Great Lakes coastal wetlands: Responding to an operational requirement. *Remote Sens.* **2020**, *12*, 3024. [CrossRef]
42. Bourgeau-Chavez, L.; Endres, S.; Battaglia, M.; Miller, M.E.; Banda, E.; Laubach, Z.; Higman, P.; Chow-Fraser, P.; Marcaccio, J. Development of a bi-national Great Lakes coastal wetland and land use map using three-season PALSAR and Landsat imagery. *Remote Sens.* **2015**, *7*, 8655–8682. [CrossRef]
43. Wolter, P.T.; Johnston, C.A.; Niemi, G.J. Mapping submergent aquatic vegetation in the US Great Lakes using Quickbird satellite data. *Int. J. Remote Sens.* **2005**, *26*, 5255–5274. [CrossRef]
44. Cvetkovic, M.; Chow-Fraser, P. Use of ecological indicators to assess the quality of Great Lakes coastal wetlands. *Ecol. Indic.* **2011**, *11*, 1609–1622. [CrossRef]
45. Eikenberry, B.C. *Summary of Biological Investigations Relating to Water Quality in the Western Lake Michigan Drainages, Wisconsin and Michigan*; US Geological Survey; US Department of the Interior: Washington, DC, USA, 1996.
46. Valenti, V.L.; Carcelen, E.C.; Lange, K.; Russo, N.J.; Chapman, B. Leveraging Google earth engine user interface for semiautomated wetland classification in the Great Lakes Basin at 10 m with optical and radar geospatial datasets. *IEEE J. Sel. Top. Appl. Earth Obs. Remote Sens.* **2020**, *13*, 6008–6018. [CrossRef]
47. Mahdavi, S.; Salehi, B.; Amani, M.; Granger, J.E.; Brisco, B.; Huang, W.; Hanson, A. Object-based classification of wetlands in Newfoundland and Labrador using multi-temporal PolSAR data. *Can. J. Remote Sens.* **2017**, *43*, 432–450. [CrossRef]
48. Amani, M.; Salehi, B.; Mahdavi, S.; Granger, J.E.; Brisco, B.; Hanson, A. Wetland classification using multi-source and multi-temporal optical remote sensing data in Newfoundland and Labrador, Canada. *Can. J. Remote Sens.* **2017**, *43*, 360–373. [CrossRef]
49. Ghorbanian, A.; Ahmadi, S.A.; Amani, M.; Mohammadzadeh, A.; Jamali, S. Application of artificial neural networks for mangrove mapping using multi-temporal and multi-source remote sensing imagery. *Water* **2022**, *14*, 244. [CrossRef]
50. Kaplan, G.; Avdan, U. Evaluating the utilization of the red edge and radar bands from sentinel sensors for wetland classification. *Catena* **2019**, *178*, 109–119. [CrossRef]

51. Mahdianpari, M.; Granger, J.E.; Mohammadimanesh, F.; Salehi, B.; Brisco, B.; Homayouni, S.; Gill, E.; Huberty, B.; Lang, M. Meta-analysis of wetland classification using remote sensing: A systematic review of a 40-year trend in North America. *Remote Sens.* **2020**, *12*, 1882. [CrossRef]
52. Drusch, M.; Del Bello, U.; Carlier, S.; Colin, O.; Fernandez, V.; Gascon, F.; Hoersch, B.; Isola, C.; Laberinti, P.; Martimort, P.; et al. Sentinel-2: ESA's optical high-resolution mission for GMES operational services. *Remote Sens. Environ.* **2012**, *120*, 25–36. [CrossRef]
53. Pahlevan, N.; Chittimalli, S.K.; Balasubramanian, S.V.; Vellucci, V. Sentinel-2/Landsat-8 product consistency and implications for monitoring aquatic systems. *Remote Sens. Environ.* **2019**, *220*, 19–29. [CrossRef]
54. Huang, H.; Roy, D.P.; Boschetti, L.; Zhang, H.K.; Yan, L.; Kumar, S.S.; Gomez-Dans, J.; Li, J. Separability analysis of Sentinel-2A Multi-Spectral Instrument (MSI) data for burned area discrimination. *Remote Sens.* **2016**, *8*, 873. [CrossRef]
55. Ranghetti, L.; Boschetti, M.; Nutini, F.; Busetto, L. "sen2r": An R toolbox for automatically downloading and preprocessing Sentinel-2 satellite data. *Comput. Geosci.* **2020**, *139*, 104473. [CrossRef]
56. Henderson, F.M.; Lewis, A.J. Radar detection of wetland ecosystems: A review. *Int. J. Remote Sens.* **2008**, *29*, 5809–5835. [CrossRef]
57. Amani, M.; Salehi, B.; Mahdavi, S.; Brisco, B. Spectral analysis of wetlands using multi-source optical satellite imagery. *ISPRS J. Photogramm. Remote Sens.* **2018**, *144*, 119–136. [CrossRef]
58. Amani, M.; Salehi, B.; Mahdavi, S.; Brisco, B. Separability analysis of wetlands in Canada using multi-source SAR data. *GIScience Remote Sens.* **2019**, *56*, 1233–1260. [CrossRef]
59. Mahdavi, S.; Salehi, B.; Amani, M.; Granger, J.; Brisco, B.; Huang, W. A dynamic classification scheme for mapping spectrally similar classes: Application to wetland classification. *Int. J. Appl. Earth Obs. Geoinf.* **2019**, *83*, 101914. [CrossRef]
60. Achanta, R.; Susstrunk, S. Superpixels and polygons using simple non-iterative clustering. In Proceedings of the IEEE Conference on Computer Vision and Pattern Recognition, Honolulu, HI, USA, 21–26 July 2017; pp. 4651–4660.
61. Tassi, A.; Vizzari, M. Object-oriented lulc classification in google earth engine combining snic, glcm, and machine learning algorithms. *Remote Sens.* **2020**, *12*, 3776. [CrossRef]
62. Movaghar, A.; Mailick, M.; Sterling, A.; Greenberg, J.; Saha, K. Automated screening for Fragile X premutation carriers based on linguistic and cognitive computational phenotypes. *Sci. Rep.* **2017**, *7*, 2674. [CrossRef] [PubMed]
63. Naboureh, A.; Ebrahimy, H.; Azadbakht, M.; Bian, J.; Amani, M. RUESVMs: An ensemble method to handle the class imbalance problem in land cover mapping using Google Earth Engine. *Remote Sens.* **2020**, *12*, 3484. [CrossRef]
64. Naboureh, A.; Li, A.; Bian, J.; Lei, G.; Amani, M. A hybrid data balancing method for classification of imbalanced training data within google earth engine: Case studies from mountainous regions. *Remote Sens.* **2020**, *12*, 3301. [CrossRef]
65. Mahdianpari, M.; Salehi, B.; Mohammadimanesh, F.; Brisco, B.; Mahdavi, S.; Amani, M.; Granger, J.E. Fisher Linear Discriminant Analysis of coherency matrix for wetland classification using PolSAR imagery. *Remote Sens. Environ.* **2018**, *206*, 300–317. [CrossRef]
66. Amani, M.; Salehi, B.; Mahdavi, S.; Brisco, B.; Shehata, M. A Multiple Classifier System to improve mapping complex land covers: A case study of wetland classification using SAR data in Newfoundland, Canada. *Int. J. Remote Sens.* **2018**, *39*, 7370–7383. [CrossRef]
67. Mahdianpari, M.; Salehi, B.; Rezaee, M.; Mohammadimanesh, F.; Zhang, Y. Very deep convolutional neural networks for complex land cover mapping using multispectral remote sensing imagery. *Remote Sens.* **2018**, *10*, 1119. [CrossRef]
68. Rezaee, M.; Mahdianpari, M.; Zhang, Y.; Salehi, B. Deep convolutional neural network for complex wetland classification using optical remote sensing imagery. *IEEE J. Sel. Top. Appl. Earth Obs. Remote Sens.* **2018**, *11*, 3030–3039. [CrossRef]
69. DeLancey, E.R.; Simms, J.F.; Mahdianpari, M.; Brisco, B.; Mahoney, C.; Kariyeva, J. Comparing deep learning and shallow learning for large-scale wetland classification in Alberta, Canada. *Remote Sens.* **2019**, *12*, 2. [CrossRef]
70. Jamali, A.; Mahdianpari, M.; Mohammadimanesh, F.; Brisco, B.; Salehi, B. 3-D hybrid CNN combined with 3-D generative adversarial network for wetland classification with limited training data. *IEEE J. Sel. Top. Appl. Earth Obs. Remote Sens.* **2022**, *15*, 8095–8108. [CrossRef]

Disclaimer/Publisher's Note: The statements, opinions and data contained in all publications are solely those of the individual author(s) and contributor(s) and not of MDPI and/or the editor(s). MDPI and/or the editor(s) disclaim responsibility for any injury to people or property resulting from any ideas, methods, instructions or products referred to in the content.